nature physics
SUPPLEMENTARY INFORMATION
DOI: 10.1038/NPHYS1774

Supplementary Online Material

Spin imaging resolution

The spin-RESOLFT signal is proportional to $f(x) = n_0(x)I_G(x)$, where n_0 is the population of the $m_s = 0$ state, $I_G = \exp(-\alpha(x/r_C)^2)$ is the intensity profile of the gaussian beam used for readout of the electronic spin, $r_C = \lambda/2\mathtt{NA}$ is the confocal resolution and $\alpha = 4/log(2)$. n_0 depends on the duration of the doughnut beam t_D; it can be evaluated by solving the rate equations of the system given in Figure S3. In the limit of large lifetime of the spin transition, it is given by $n_0 = \exp(-R_x t_D)$, where $R_x = \epsilon k_x$ is the position-dependent optical depletion rate out of the $m_s = 1$ state (i.e., polarization rate to the $m_s = 0$ state measured after waiting for the non-radiative relaxation from the singlet state to the $m_s = 0$ state), k_x is the intensity profile of the doughnut-shaped beam and ϵ is the branching ratio of the spin changing ($m_s = 1 \rightarrow m_s = 0$) decay relative to the total decay of the excited state. In the unsaturated regime, $R_x = R_0 + \alpha\Gamma(x/r_C)^2$, where $\Gamma = \kappa\epsilon$ is proportional to the optical excitation rate associated with the maximal intensity of the doughnut κ, and $R_0 = \epsilon\kappa_0$ is proportional to the intensity of the doughnut center and the corresponding excitation κ_0. The resolution r is defined by $f(x) = \exp(-\alpha(x/\Delta r)^2)$. Solving for Δr leads to Eq. (1) in the main text. In the case of a perfect doughnut beam the ultimate resolution is determined by the maximum values of $\Gamma = \gamma\epsilon$ and $T_D \sim T_1$. Thus leading to an improvement in resolution relative to the diffraction limit of a confocal microscope of $\sqrt{\epsilon\gamma T_1}$.

In our experiments, the resolution is limited by a small imperfection of the doughnut-zero intensity. We can find the maximum achievable resolution by using a model that includes a back pumping process which brings the electronic spin from the $m_s = 0$ to the $m_s = 1$ state, and finite spin lifetime. Consider the rate equations of our two level system ($m_s = 0$ and $m_s = 1$),

$$\frac{dn_0}{dt} = R_x n_1 - \gamma_{0\rightarrow 1}(n_1 - n_0) \tag{1}$$

and $n_1 = 1 - n_0$. The solution for this equation is,

$$n_1 = \frac{\gamma_1 + R_x}{2\gamma_{0\rightarrow 1} + R_x}(1 - e^{-(2\gamma_{0\rightarrow 1} + R_x)t_D}) \tag{2}$$

The resolution δr is defined by the FWHM condition $n_2(R_{r/2}, t) = \frac{1}{2}n_2(R_0, t)$. The maximum improvement in resolution relative to the diffraction limit of a confocal microscope is given

DOI: 10.1038/NPHYS1774

by

$$\Delta r/r_C = \sqrt{R_0/\Gamma}\sqrt{1+2\gamma_{0\to1}/R_0} \tag{3}$$

for an optimal doughnut duration $t_D = \log[(3\gamma_{0\to1}+2R_0)/(\gamma_{0\to1}+R_0)]/(2\gamma_{0\to1}+R_0)$, where $\gamma_{0\to1}$ is the total rate out of the electronic spin $m_s = 0$. In the limit of long spin lifetime ($\gamma_{0\to1} \ll R_0$), the maximum improvement in resolution is given by $\sqrt{R_0/\Gamma} = \sqrt{\kappa_0/\kappa}$, i.e., the intensity of the doughnut center relative to the maximum doughnut intensity. In our experiments, $\kappa_0/\kappa \approx 1\%$, which is in a good agreement with our 10-fold improvement in resolution relative to the diffraction limit.

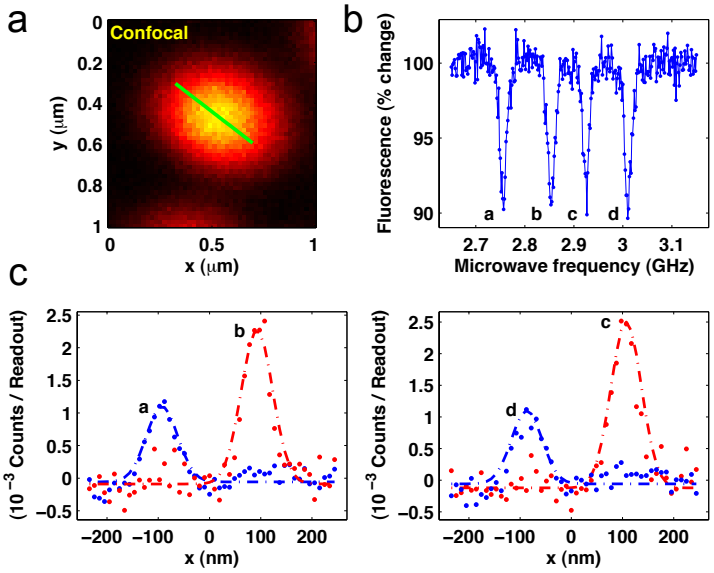

Figure S1. Demonstration of sub-diffraction optical imaging of neighbouring NV centers. A Closely spaced NV centers cannot be resolved using conventional standard imaging. B Optically-detected ESR spectrum with an applied DC magnetic field of 60 G indicates presence of two NV centers with different crystallographic orientations. C Individual NV centers are imaged with sub-diffraction resolution by scanning along the trajectory indicated in A. Each 1D image is obtained by selectively driving corresponding ESR resonance (A-D) with resonant microwave pulse followed by application of doughnut beam and optical readout. Each ESR spectral signature is thereby uniquely associated with its spatial location. Resonances a,c correspond to $|0\rangle \to |\pm 1\rangle$ transitions of one NV center, while resonances b,d are corresponding transitions for a second NV center.

To demonstrate the nanoscale resolving power of our spin sensitive far-field optical technique, we imaged NV centers in bulk diamond separated by less than the diffraction limit.

Figure S1a shows a pair of individual NV centers that cannot be resolved using confocal microscopy. However, an optically detected ESR measurement performed in this location displays multiple spectral lines (Figure S1b), indicating the presence of multiple NV centers with different crystallographic orientations relative to the applied static magnetic field. Using our sub-diffraction spin detection technique and scanning the microwave frequency, we associated each ESR spectral line with the corresponding location of an individual NV center with sub-diffraction limited resolution (Figure S1c). In particular, sub-diffraction spin imaging scans along the trajectory indicated in Figure S1a, taken for each ESR transition frequency, reveal that two NV centers are responsible for the observed ESR spectrum: each NV center has two spectral ESR lines corresponding to the $|0\rangle \rightarrow |+1\rangle$ and $|0\rangle \rightarrow |-1\rangle$ transitions.

DOI: 10.1038/NPHYS1774

Measurements of local magnetic field environment with sub-diffraction resolution

As described in the main text, individual NV centers can be resolved, independently manipulated and read-out using our technique. Here we individually measure the response of two NV centers to their local magnetic environment using Rabi and spin-echo techniques. By placing the center of the doughnut over one NV center, the other NV center is polarized and only contributes a constant background to the fluorescence signal. Figure S2 shows the raw data for Rabi measurements of the two NV centers in Figure 3 when the doughnut zero is placed over Center 1 (upper-left panel) and Center 2 (bottom-left panel). When the two curves are added together (green line, right panel), the confocal measurement (taken at the position of Center 1) is recovered (dotted line in Figure S2).

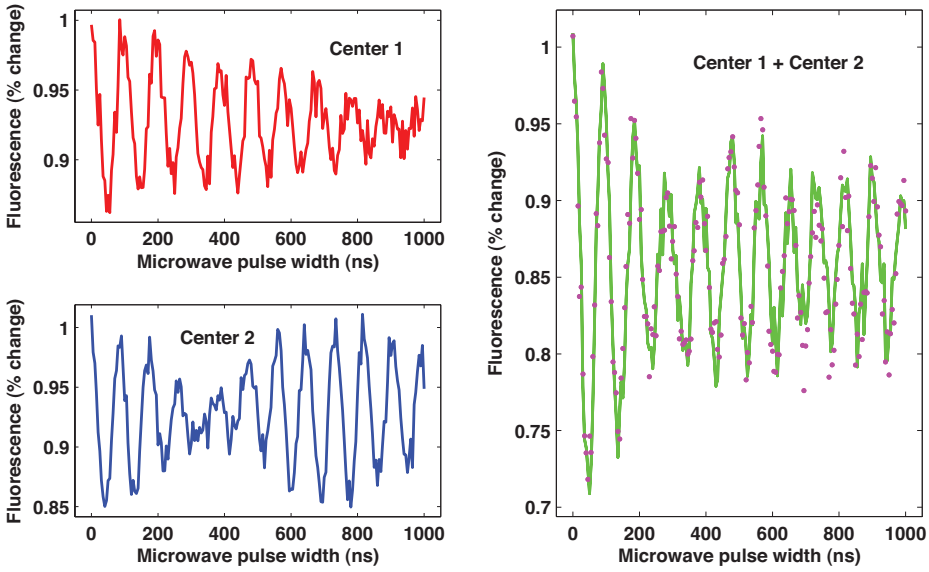

Figure S2. Realization of spin-RESOLFT Rabi measurements. Rabi oscillations for each NV center were measured by centering the doughnut on one of the NV centers. The addition of the two Rabi oscillation data curves (green line, right panel) corresponds to the confocal measurement of both NV centers as expected (pink dots, right panel).

The observed modulations of the Rabi oscillations shown in Figure 3c (and Figure S2) reveal the different magnetic fields experienced by each NV center. These modulations are caused by hyperfine induced splitting in the NV center's electronic transition ($m_s = 0 \rightarrow 1$)

associated with the ^{15}N nuclear spin ($I = \frac{1}{2}$). A simple model for the probability of finding the electronic spin in the $m_s = 0$ state, P_0, assumes that on average the ^{15}N nuclear spin is half of the time in its spin down state and the other half of the time in its spin up state. Thus, P_0 is just the average of the dynamics of two two-level systems with different splittings. For a two-level system with states $|0\rangle$ and $|1\rangle$, Rabi frequency Ω and detuning δ, the probability to find the system in state $|1\rangle$ (starting from state $|0\rangle$) is given by $(\frac{\Omega}{\Omega_e})^2 \sin^2 \Omega_e \tau$, where $\Omega_e^2 = \Omega^2 + \delta^2$. Therefore, P_0 in our case is given by

$$P_0 = \frac{1}{2}\left(2 - \left(\frac{\Omega}{\Omega_1}\right)^2 \sin^2(\Omega_1 \tau/2) - \left(\frac{\Omega}{\Omega_2}\right)^2 \sin^2(\Omega_2 \tau/2)\right) \tag{4}$$

where $\Omega_1^2 = \Omega^2 + \delta_1^2$ and $\Omega_2^2 = \Omega^2 + \delta_2^2$. If $\Omega \gg \delta$, the modulation frequency is given by $\Delta\Omega = \Omega_2 - \Omega_1 \approx (\delta_1 + \delta_2)(\delta_1 - \delta_2)/2\Omega$. Since $\delta_1 + \delta_2 = 2(f_0 - f)$ and $\delta_2 - \delta_1 = A$, the modulation frequency for an NV center is given by $\Delta\Omega = (\nu_0 - \nu)A/\Omega$, where ν_0 is the frequency of the electronic transition $m_s = 0 \rightarrow 1$, ν is the microwave frequency and $A = 3.05$ MHz[1] is the hyperfine splitting induced by the ^{15}N nuclear spin present on each of our NV centers (see section Samples).

Modulations appear when the microwave frequency is detuned from the central transition $\nu_0^i = \Delta + \gamma_e B^i$, where B^i is the local magnetic field along the NV axis of center i, Δ is the zero-field splitting, and γ_e is the gyromagnetic ratio of the electronic spin. In other words, modulations appear when the two hyperfine transitions are driven with different detunings. The difference in the modulation frequencies of each NV center ($\Delta\Omega_2 - \Delta\Omega_1 = 1.3 - 0.5 = 0.8$ MHz) reveals a difference in the static magnetic field experienced by each NV center of about $\Delta B = 1$ G.

Spin echo measurements can reveal even more subtle differences in the local environment between the two NV centers. In our measurements (Figure 3d), the dominant contribution comes from interactions between the electronic spin of the NV center and the ^{15}N nuclear spin and ^{13}C nuclear spin bath. The spin echo signal can be written as [2] $p(\tau) = \frac{1+S(\tau)}{2}$, where $S(\tau)$ is the pseudo spin which can be written as the multiplication of all individual nuclear spin contributions. The first collapse and first revival of the NV spin echo signal can thus be approximated by

$$S(\tau) = S_{^{15}N}(\tau)\left(e^{-(\tau/\tau_C)^4} + ce^{-((\tau-\tau_R)/\tau_C)^4}\right), \tag{5}$$

where we have phenomenologically grouped the effect of all ^{13}C nuclear spins in the expo-

DOI: 10.1038/NPHYS1774

nential decays, and where τ_C is the collapse rate[2] given by $\tau_C = 13\mu\mathrm{s}\sqrt{\frac{5\mathrm{G}}{B}}$, B is the local magnetic field, τ_R is the revival time, c is the contrast of the first revival. The pseudo spin for the ^{15}N nuclear spin is given by

$$S_{^{15}N}(\tau) = 1 - \frac{|\Omega_{^{15}N,0} \times \Omega_{^{15}N,1}|^2}{|\Omega_{^{15}N,0}|^2|\Omega_{^{15}N,1}|^2} \sin(\Omega_{^{15}N,0}\tau/2)^2 \sin(\Omega_{^{15}N,1}\tau/2)^2, \tag{6}$$

where $\Omega_{^{15}N,m_s}$ is the Larmor frequency of ^{15}N when the electron is in state m_s. The blue lines in Figure 3d are fitted to equation (5). While Center 2 shows good coherence ($c = 0.86$), Center 1 shows no revival of the signal ($c = 0$). The absence of revival for Center 1 can be due to an unfavorable distribution of nearby pairs of ^{13}C nuclear spins that quickly decohere the electronic spin [23], or due to nearby paramagnetic impurities or other defects. The position of the first revival for Center 2, $\tau_R = 13.5$ μs, is set by the Larmor precession of ^{13}C, $\tau_R^{-1} = \omega_{C13} = \gamma_{C13}B$, corresponding to a local magnetic field of B = 69 G. The high frequency oscillations ($\Omega_{^{15}N,1}$) correspond to the hyperfine interaction between the electronic spin and the ^{15}N nuclear spin, $\Omega_{^{15}N,1} \approx A = 3.05$ MHz. Meanwhile the slow frequency component of the dynamics, $\Omega_{^{15}N,0} = 360$ kHz, corresponds to the Larmor frequency of the ^{15}N nuclear spin when the electron is in state $m_s = 0$. We immediately notice that the slow frequency component is too large to be explained by the bare Larmor frequency of ^{15}N at 69 G, $\gamma_{N15}B = 30$ kHz. This slow frequency component $\Omega_{^{15}N,0}$ is enhanced by virtual transitions between the NV electronic spin and the ^{15}N nuclear spin. To understand this effect, we first introduce the following Hamiltonian that governs the dynamics,

$$H = \Delta S_z^2 - \gamma_e B \cdot S - \gamma_n B \cdot I - S \cdot A \cdot I \tag{7}$$

where $\Delta = 2.87$ GHz is the zero field splitting, γ_e (γ_n) is the electronic (nuclear) gyromagnetic ratio, B is the magnetic field and A is the hyperfine tensor. This Hamiltonian leads to very interesting effects such as enhancement of the g-factor [2] and assisted interaction between nearby nuclei [5]. Here we only analyze the relevant effect for our experiments, the enhancement of the g-factor. In the spirit of second order perturbation theory, we can divide Hamiltonian (7) in two parts, the secular part

$$H_0 = \Delta S_z^2 - \gamma_e B_z S_z - \gamma_n B \cdot I - S_z A_z \cdot I \tag{8}$$

and the non-secular part

$$V = -\gamma_e(B_x S_x + B_y S_y) - (S_x A_x + S_y A_y) \cdot I. \tag{9}$$

By using perturbation theory to second order, we can determine that the enhancement in the interaction between the magnetic field and the nuclear spin can be written as $B \cdot \Delta g \mu_N / \hbar \cdot I$, where μ_N is the nuclear magneton and Δg is the enhanced g-tensor given by

$$\Delta g = -(3|m_s| - 2)\frac{g_n \gamma_e}{\Delta \gamma_n} \begin{pmatrix} A_{xx} & A_{xy} & A_{xz} \\ A_{yx} & A_{yy} & A_{yz} \\ 0 & 0 & 0 \end{pmatrix} \tag{10}$$

In the case of ^{15}N, the hyperfine interaction is isotropic[1] and the enhancement is given by $\Delta g^0 \approx 7.8$ (corresponding to a gyromagnetic increment factor of $2(\gamma_2/\gamma_n)A/\Delta \approx 14$). Therefore, $\Omega_{^{15}N,0} \approx 14\gamma_n B_\perp$ corresponding to a perpendicular field to the NV axis of $B_\perp = 60$ G. This value is in agreement with the component of the magnetic field parallel to the NV axis that leads to the observed splitting in the ESR spectrum (Figure 3a), $B_{||} = 36$ G ($B = \sqrt{36^2 + 59^2} \approx 69$ G).

DOI: 10.1038/NPHYS1774

Inhibition of Electronic-Spin Rabi Oscillations

In this section, we describe in detail the optical inhibition of electronic spin Rabi oscillations using a doughnut beam (Figure 4b in the main text). The basic idea can be explained by considering a simple two-level system (with states $|0\rangle$ and $|1\rangle$), which undergoes Rabi oscillations (with Rabi frequency Ω) and which is subject to an effective dephasing (with dephasing rate γ_p). The system dynamics is then governed by the Hamiltonian $H = -\frac{\Omega}{2}\sigma_x$ (where $\vec{\sigma}$ are Pauli matrices) combined with the decay of the off-diagonal matrix elements of the density matrix ρ with rate γ_p. Formally, this is described by the following master equation:

$$\frac{d\rho}{dt} = i\left[\frac{\Omega}{2}\sigma_x, \rho\right] - \frac{\gamma_p}{4}\left[\sigma_z, [\sigma_z, \rho]\right]. \tag{11}$$

Suppose the system starts in the $|0\rangle$ state, i.e., $P_0(t=0) = 1$. We analytically solve the master equation and obtain the probability of being in the $|0\rangle$ state as a function of time:

$$P_0(t) = \frac{1}{2}\left(1 + \frac{\Gamma_+ e^{-\Gamma_- t} - \Gamma_- e^{-\Gamma_+ t}}{\Gamma_+ - \Gamma_-}\right), \tag{12}$$

where $\Gamma_\pm = \frac{1}{2}\left(\gamma_p \pm \sqrt{\gamma_p^2 - 4\Omega^2}\right)$. We may also use the approximate form:

$$P_0(t) \approx \begin{cases} \frac{1}{2}\left(1 + \cos(\Omega t)\, e^{-\gamma_p t/2}\right) & \text{for } \Omega \gg \gamma_p \\ \frac{1}{2}\left(1 + \exp\left(-\frac{\Omega^2}{\gamma_p} t\right)\right) & \text{for } \Omega \ll \gamma_p \end{cases}. \tag{13}$$

For $\Omega \gg \gamma_p$, the two-level system undergoes Rabi oscillations with an amplitude decay rate $\gamma_p/2$. This scenario approximately describes the evolution of Center 1 [blue curve in Figure 4b in the main text]: there the amplitude decay comes from a combination of T_2^* decay and of the dephasing due to the imperfect zero of the doughnut. On the other hand, for $\Omega \ll \gamma_p$, the oscillation dynamics is inhibited, and the system remains in the initial state $|0\rangle$ with a slow spin-relaxation rate Ω^2/γ_p, which is inversely proportional to γ_p. This scenario, which we refer to as a quantum Zeno-like effect [4], approximately describes the evolution of Center 2 [green curve in Figure 4b in the main text]. In particular, the scheme succeeds if the spin-relaxation rate in Center 2 over the course of a π-pulse on Center 1 is much less than unity: $1 - P_0(t) \approx (1/2)(\Omega^2/\gamma_p) * (\pi/\Omega) = \pi\Omega/(2\gamma_p) \ll 1$. In other words, for times $t \ll \gamma_p/\Omega^2$ the center is "frozen" in the ground state.

In reality, the experimental situation is more complicated than this simple two-level model. Specifically, we must account for processes in which the spin is first flipped to

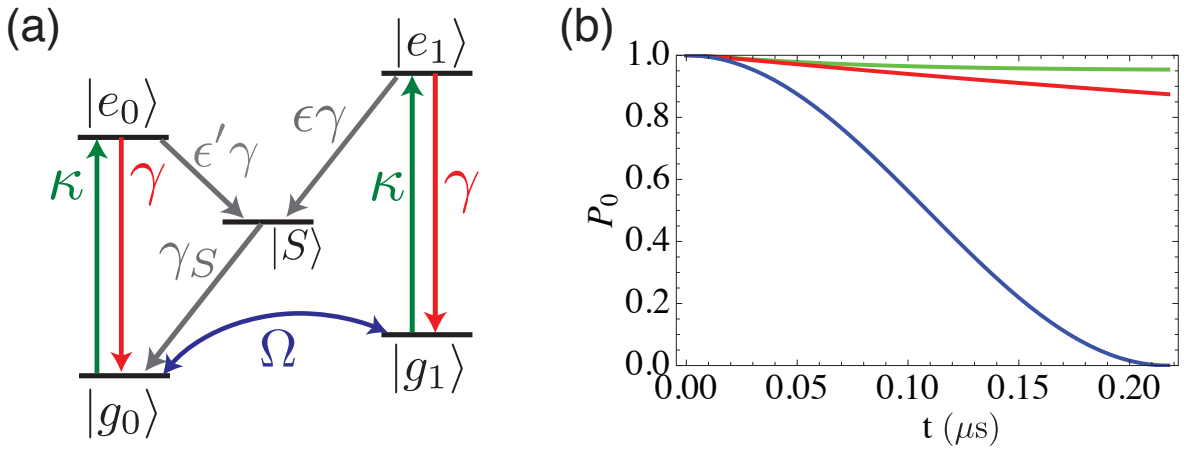

Figure S3. (a) 5-level system used to model inhibition of electronic-spin Rabi oscillations. $\gamma \approx 1/(13\text{ ns}) = (2\pi)12.2$ MHz, $\gamma_S \approx 1/(300\text{ ns})$, and $\Omega = (2\pi)2.3$ MHz. (b) Calculated inhibition of electronic-spin Rabi oscillations: the blue curve has $\kappa = 0$ and shows an uninhibited Rabi π-pulse [analogous to Center 1 evolution shown as the blue curve in Figure 4b of the main text]; the green (red) curve has $\kappa = \gamma$ and $\epsilon = 0.3$ ($\epsilon = 0$), $\epsilon' = 0$ and demonstrates the inhibition of the Rabi oscillations. The green curve is analogous to Center 2 evolution shown as the green curve in Figure 4b of the main text. The fact that the red curve stays close to 1 confirms that the quantum Zeno-like effect due to dephasing (and not the optical pumping from $|g_1\rangle$ to $|g_0\rangle$) plays a dominant role in suppressing Rabi oscillations of Center 2. The value (here ≈ 0.9) of the red curve at the final time π/Ω can be used as a rough estimate of preservation of nuclear spin coherence on Center 2 in future experiments.

state $|1\rangle$ and subsequently repolarized to state $|0\rangle$. We therefore model the experiment by considering the five-level system shown in Figure S3(a). The five states are the ground states $|g_0\rangle$ with $m_s = 0$ and $|g_1\rangle$ with $m_s = 1$, the excited states $|e_0\rangle$ with $m_s = 0$ and $|e_1\rangle$ with $m_s = 1$, as well as the singlet $|S\rangle$. In addition to the coherent evolution with Rabi frequency Ω, the system is subject to incoherent excitation (caused by the green laser) from the ground to the excited states with rate κ. Moreover, the excited states decay down to the triplet with rate $\gamma \approx 1/(13\text{ ns}) = (2\pi)12.2$ MHz [3]. At the same time, the state $|e_1\rangle$ decays down to the singlet with rate $\epsilon\gamma$, where we take $\epsilon = 0.3$, while the singlet decays to $|g_0\rangle$ with rate $\gamma_S \approx 1/(300\text{ ns})$. After extracting $\Omega = (2\pi)2.3$ MHz from the uninhibited Rabi oscillations of Center 1 [Figure 4b in the main text] and $\kappa \approx \gamma$ (on Center 2) from the fluorescence

DOI: 10.1038/NPHYS1774

saturation curve (not shown), we know all the parameters and can compute the resulting evolution of Center 2 over time π/Ω, which is sufficient for a π pulse on the uninhibited Center 1. We begin with Center 2 in the state $|g_0\rangle$, keep the microwave and the green light on for time t, then allow the population to relax to $|g_0\rangle$ and $|g_1\rangle$, and plot in green in Figure S3(b) the resulting population P_0 of $|g_0\rangle$ for Center 2 as a function of t. In agreement with the green curve in Figure 4b of the main text, we see that the population stays within a few percent of the initial population of unity, while Center 1 (with $\kappa \approx 0$) does a Rabi π pulse (blue curve). The reason why the blue curve in Figure 4b of the main text does not show a perfect π-pulse is because the doughnut zero is imperfect and because T_2^* is finite.

To confirm that the observed inhibition indeed comes largely from Zeno-like effects and not from re-pumping of the electronic spin from $|g_1\rangle$ to $|g_0\rangle$ via the singlet, we plot in red in Figure S3(b) the equivalent of the green curve except with $\epsilon = 0$, i.e. we turn off the $|g_1\rangle \rightarrow |g_0\rangle$ pumping process. We observe that the population still stays mostly in $|g_0\rangle$, confirming that it is indeed Zeno-like dynamics that are largely responsible for the inhibition. In fact, for our parameters ($\kappa \gg \Omega$), the red curve has a simple analytical form

$$P_0(t) = \frac{1}{2}\left(1 + e^{-\frac{\gamma}{\kappa+\gamma}\frac{\Omega^2}{\kappa}t}\right). \tag{14}$$

Since both $|g_0\rangle$ and $|g_1\rangle$ are excited with rate κ, the coherence between these two levels decays with rate κ, so κ plays the role of the dephasing rate γ_p from our two-level model above. The prefactor $\gamma/(\kappa+\gamma)$ in front of Ω^2/κ is the population that is in the ground state triplet, while the remainder is in the excited state and is unaffected by Ω since the corresponding transition in the excited state is highly off-resonant (and was, thus, not included in the model). Under this approximation, the transition probability for Center 2 over time π/Ω is $1 - P_0(t) \approx [\gamma/(\kappa+\gamma)][\pi\Omega/(2\kappa)]$, which for our parameters is ≈ 0.1, which is much smaller than unity, as desired. This value can be further reduced by going to larger green laser powers or smaller Rabi frequencies. In addition, if strain and an off-axis magnetic field are included, population transfer from $|e_0\rangle$ to the singlet $^1A_1$ is possible, allowing a further suppression of coherent spin manipulation via the microwave field.

In Figure 4a we verify this suppression experimentally by studying a single isolated NV center using the pulse sequences S1 and S2. Our analysis requires knowledge of the populations ($\rho_{0,0}$, $\rho_{1,1}$, $\rho_{S,S}$) of the $m_s = 0$, $m_s = \pm 1$ and $^1A_1$ manifolds right after state

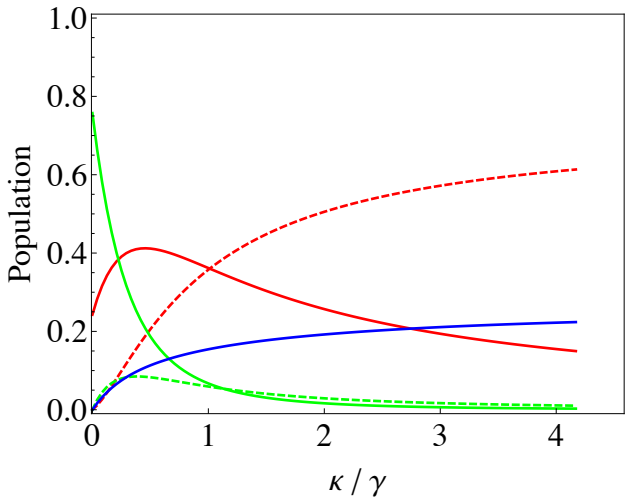

Figure S4. Estimated population in the $|g_0\rangle$ (solid red), $|e_0\rangle$ (dashed red), $|g_1\rangle$ (solid green), $|e_1\rangle$ (dashed green) and $^1A_1$ (blue) state as a function of optical excitation power. The calculations are based on the master equation found in figure 4a of the main text.

preparation. To determine these quantities, we record the fluorescence f

$$f(\tau_d) = f^0\rho_{0,0}(\tau_d) + f^1\rho_{1,1}(\tau_d)$$

of a single NV center for two different times $\tau_d \ll T_S$ and $\tau_d \gg T_S$; where τ_d is the time defined in S1 and S2 of Figure 4a; $T_S = 300$ ns is the lifetime of the singlet $^1A_1$; and f^{m_S} are the fluorescence rates for the corresponding states, which can be determined experimentally. Since the singlet $^1A_1$ nearly always decays non-radiatively into the $m_s = 0$ state[3] we can extract the populations $\rho_{i,i}$, which are shown in Figure 4a, from measuring the fluorescence at $\tau_d \ll T_S$ and $\tau_d \gg T_S$ and using the relation $\rho_{0,0} + \rho_{1,1} + \rho_{S,S} = 1$.

To investigate the mechanism for the observed inhibition of coherent spin transitions in the presence of a resonant microwave field, we fit the extracted population of the $m_s = 0$, $m_s = 1$ manifold and $^1A_1$ state to the solution of a master equation, which additionally includes the hyperfine levels of ^{15}N. The fit parameters include the optical excitation rate κ, the branching ratio ϵ from the $|e_1\rangle$ to the $^1A_1$ state, and the branching ratio ϵ' from the $|e_0\rangle$ to the $^1A_1$ state.

To evaluate the individual contribution for each of these three effects, we calculate the population in $|g_0\rangle$, $|e_0\rangle$, and $^1A_1$ using the transition rates found in Figure 4a of the main text, which are shown in Figure S4. From this calculation, we conclude that inhibition of

DOI: 10.1038/NPHYS1774

spin transitions at large optical pumping powers is mainly due to population hiding in the $|e_0\rangle$ state; while suppression at small optical pumping is mostly caused by the quantum Zeno effect. For the typical parameters of our experiment (Figure 4b), both effects contribute to the suppression of coherent spin transitions.

One eventual goal of this demonstrated inhibition is to allow quantum information stored in a nuclear spin degree of freedom (coming from the nitrogen or a nearby carbon-13) to be controllably manipulated in each NV center. Provided that the electron state of the illuminated NV center (Center 2) is kept in $|m_s = 0\rangle$, the state of the corresponding nuclear spin would be preserved [5], while the nuclear spin associated with Center 1 can be prepared, coherently manipulated, or detected with sub-wavelength resolution. The performance of this technique can be directly evaluated from our measurements. Specifically, the error induced on the nuclear spin associated with illuminated Center 2 is proportional to $1 - P_0 \approx 0.1 \ll 1$. This small error indicates that the state of the nuclear spin associated with Center 2 can be well preserved while we manipulate Center 1.

Measurement of individual spin states in coherent manipulation experiments

In Figure 4b of the main text, we demonstrate that a green doughnut-shaped laser beam inhibits electronic-spin Rabi oscillations for one of two NV centers separated by 150 nm. As seen in this figure, NV Center 1, which sits at the zero intensity point of the doughnut, undergoes spin Rabi oscillations; while Center 2, sitting outside the center of the doughnut, remains in the $m_S = 0$ state. In order to probe this behavior, two experiments (pulse sequences S3 and S4 in Figure 4b) were performed to extract the probability of each center remaining in the initial state $m_s = 0$, as explained in the main text. Here we present the details of our analysis.

Intuitively, the experimental sequence S3 results in the readout of both spin states simultaneously, while the experimental sequence S4 (involving spin-RESOLFT readout) results in the detection of Center 1 alone.

The fluorescence of Center i is given by $f_i = f_i^0 p_i(0) + f_i^1 p_i(1)$, where $f_i^0 (f_i^1)$ is the fluorescence level detected when Center i is in the state $m_s = 0 (m_s = 1)$ and $p_i(m_S)$ is the probability of Center i being in state m_S. For the experiments considered in Figure 4b of the main text, the measured total level of fluorescence during the readout is $f = f_1 + f_2$.

For the experimental sequences S3 and S4,

$$f^{S3} = f_1^0 p_1^{S3}(0) + f_1^1 p_1^{S3}(1) + f_2^0 p_2^{S3}(0) + f_2^1 p_2^{S3}(1) \quad (15)$$

$$f^{S4} = f_1^0 p_1^{S4}(0) + f_1^1 p_1^{S4}(1) + f_2^0 p_2^{S4}(0) + f_2^1 p_2^{S4}(1), \quad (16)$$

where $p_i^{Sn}(m_S)$ is the probability that Center i is in state m_S after experiment Sn (prior to readout). In experiment S4, the effect of the second doughnut pulse is to polarize completely the state of Center 2. As a result, $p_2^{S4}(0) = 1$ and $p_2^{S4}(1) = 0$. In addition, an imperfect doughnut has the undesired effect of partially repolarizing Center 1. This partial repolarization is quantified by a parameter α; so that the probabilities $p_1^{S4}(m_S)$ can be expressed in terms of $p_1^{S3}(m_S)$ (the probabilities resulting from sub-wavelength coherent manipulation experiments) as follows,

$$p_1^{S4}(0) = p_1^{S3}(0) + (1-\alpha)p_1^{S3}(1) \qquad p_1^{S4}(1) = \alpha p_1^{S3}(1). \quad (17)$$

Equations (15) and (16) are then reduced to

$$f^{S3} = (f_1^0 - f_1^1)p_1^{S3}(0) + (f_2^0 - f_2^1)p_2^{S3}(0) \quad (18)$$

$$f^{S4} = f_1^0 p_1^{S3}(0) + (1-\alpha) f_1^0 p_1^{S3}(0) + \alpha f_1^1 p_1^{S3}(1) + f_2^0. \quad (19)$$

From this set of equations, we extract $p_1^{S3}(0)$ and $p_2^{S3}(0)$ as follows,

$$p_1^{S3}(0) = \frac{f^{S4} - f_1^0(1-\alpha) - \alpha f_1^1 - f_2^0}{\alpha(f_1^0 - f_1^1)} \quad (20)$$

$$p_2^{S3}(0) = 1 + \frac{\alpha f_T^{S3} - f_T^{S4}}{\alpha(f_2^0 - f_2^1)} + \frac{(1-\alpha)(f_2^0 + f_1^0)}{\alpha(f_2^0 - f_2^1)}, \quad (21)$$

which are plotted in Figure 4b of the main text.

In order to evaluate the fluorescence parameters $f_i^{m_S}$ and the parameter α, we performed an auxiliary experiment where the repolarization rates of each center due to the doughnut beam were determined. In this experiment, the doughnut beam was centered at Center 1 and both NV centers were prepared in the $m_S = 1$ state by applying a resonant π pulse, followed by repolarization with a doughnut pulse of variable duration τ and subsequent fluorescent spin dependent state detection using a Gaussian excitation beam (see Figure S5).

The fluorescence rate f in this experiment is again proportional to the projections $p_{1,2}(0)$ onto the $m_S = 0$ state of both NV centers,

$$f = f_1^0 p_1(0) + f_1^1 p_1(1) + f_2^0 p_2(0) + f_2^1 p_2(1). \quad (22)$$

DOI: 10.1038/NPHYS1774

The projection onto the $m_S = 0$ state can be written as $p_i(0) = 1 - \epsilon e^{-R_i \tau}$, where R_i is the rate of repolarization of Center i, τ the duration of the doughnut pulse and ϵ account for the imperfections of the initial π pulse. The probability for Center 1 in sequence S3 is modeled by $p_1^{S3}(0) = \frac{1}{2}\left(1 + e^{-\lambda_1 \tau} \cos \Omega_1 \tau\right)$, where Ω_1 is the Rabi frequency and λ_1 is a parameter that describes the effect of T_2^*. By using the least squares fitting of the fluorescence measurements of experiments S3, S4, and the auxiliary experiments to equations (18), (19) and (22), we obtain the following parameters: $f_1^0 = f_T^0 - f_2^0 = 0.0057(\pm 0.00002)$, $f_1^1 = f_T^1 - f_2^1 = 0.0044(\pm 0.00001)$, and $\alpha = 0.743(\pm 0.018)$, where $f_T^0 = 0.0088(\pm 0.00003)$ and $f_T^1 = 0.0064(\pm 0.00002)$ are the total level of fluorescence when the centers are in their electronic spin $m_S = 0$ and $m_S = 1$, respectively.

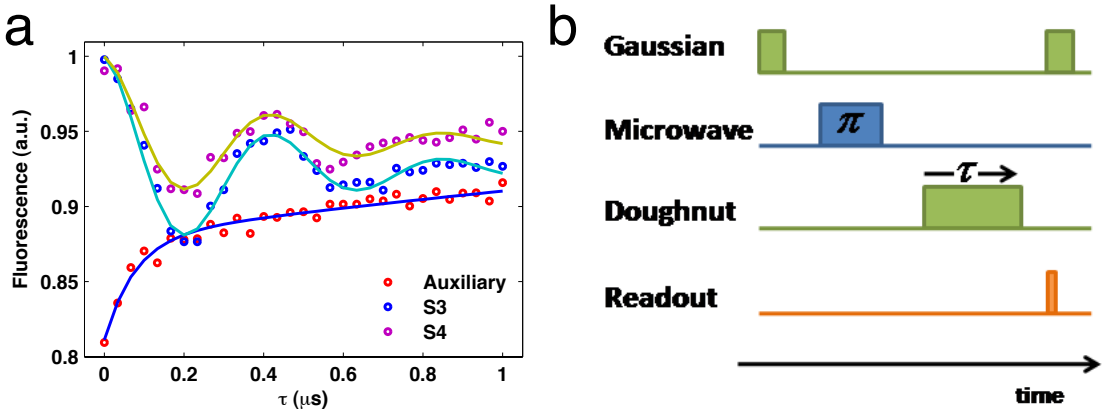

Figure S5. (a) Measured fluorescence signal for the experimental sequences S3, S4 and auxiliary as a function of the doughnut duration. Solid lines represent fittings using Equations (18), (19) and (22), respectively. (b) Schematic pulse sequence used to record the data for the auxiliary experiment.

[1] J. R. Rabeau, P. Reichart, G. Tamanyan, D. N. Jamieson, S. Prawer, F. Jelezko, T. Gaebel, I. Popa, M. Domhan, and J. Wrachtrup, "Implantation of labelled single nitrogen vacancy centers in diamond using ^{15}N", Appl. Phys. Lett. 88, 023113 (2006).

[2] L. Childress, M. V. Gurudev Dutt, J. M. Taylor, A. S. Zibrov, F. Jelezko, J. Wrachtrup, P. R. Hemmer, and M. D. Lukin, "Coherent Dynamics of Coupled Electron and Nuclear Spin Qubits in Diamond", Science 314 (5797), 281.

[3] N. B. Manson, J. P. Harrison, and M. J. Sellars, "Nitrogen-vacancy center in diamond: Model of the electronic structure and associated dynamics", Phys. Rev. B **74**, 104303 (2006).

[4] W. M. Itano, D. J. Heinzen, J. J. Bollinger, and D. J. Wineland, "Quantum Zeno effect", Phys. Rev. A **41**, 2295 (1990).

[5] L. Jiang, M. V. Gurudev Dutt, E. Togan, L. Childress, P. Cappellaro, J. M. Taylor, and M. D. Lukin, "Coherence of an Optically Illuminated Single Nuclear Spin Qubit", Phys. Rev. Lett. **100**, 073001 (2008).